X-591-73-281
PREPRINT

NASA TM X- 70608

NASA-GSFC IONOSPHERIC CORRECTIONS TO SATELLITE TRACKING DATA

P. E. SCHMID
R. B. BENT
S. K. LLEWELLYN
G. NESTERCZUK
S. RANGASWAMY

DECEMBER 1973

GSFC
GODDARD SPACE FLIGHT CENTER
GREENBELT, MARYLAND

X-591-73-281

NASA-GSFC IONOSPHERIC CORRECTIONS TO SATELLITE TRACKING DATA

P. E. Schmid
R. B. Bent
S. K. Llewellyn
G. Nesterczuk
S. Rangaswamy

December 1973

Goddard Space Flight Center
Greenbelt, Maryland

NASA-GSFC IONOSPHERIC CORRECTIONS TO SATELLITE TRACKING DATA

ABSTRACT

The purpose of this report is to present an overview of the development, verification, and recent implementation of the NASA-GSFC ionospheric model for satellite tracking data corrections. This highly successful model has been incorporated into the Goddard Trajectory Determination System which is providing continuous trajectory computation support for the lunar orbiting Radio Astronomy Explorer-B launched on 10 June 1973.

NASA-GSFC IONOSPHERIC CORRECTIONS TO SATELLITE TRACKING DATA

SUMMARY

The Earth's ionosphere introduces systematic perturbations to all radio tracking data. At present NASA radio tracking is conducted in the approximate frequency range of 140 MHz to 6 GHz. At the lower frequencies daytime ionospheric biases can easily reach several kilometers in range, several meters per second in range rate, and up to two or three milliradians in angle. At the higher frequencies these values decrease as the inverse square of frequency. However in all cases this ionospheric bias is greater than the basic tracking system resolutions involved (e.g. ref. 1). The lower tracking frequencies are preferred from the standpoint of simplified antenna pointing and hence ease of signal acquisition. The higher frequencies are preferred from the standpoint of high telemetry data rates and extremely precise orbit computation such as associated with satellite geodesy.

This report describes the general development and salient features of the highly successful ionospheric correction model incorporated into the recently completed Goddard Trajectory Analysis Program (GTDS) which eventually will provide operational support for all GSFC missions. The Radio Astronomy Explorer-B (RAE-B) launch in June 1973 was the first of the series of NASA missions to be supported by GTDS. RAE-B is being tracked by the VHF (136 - 148 MHz) Goddard Range and Range Rate System and ionospheric corrections to all tracking measurements are being automatically applied on a continuous basis. These corrections are a function of predicted solar activity, tracking station latitude and longitude, universal time and station to spacecraft geometry.

CONTENTS

NASA-GSFC IONOSPHERIC CORRECTIONS TO SATELLITE TRACKING DATA

1.0 EVOLUTION OF IONOSPHERIC RESEARCH

Over the past fifty years thousands of reports and technical papers have been compiled regarding radio wave propagation phenomena as influenced by the Earth's ionosphere. The "non-exhaustive" bibliography (cited as Ref. 2) lists 1404 references for the period 1923 to 1960 alone. In addition basic ionospheric theoretical considerations have been documented in hundreds of excellent books such as represented by references 3 through 5.

Since the early days of radio (Circa 1925) ionospheric research has had practical application in terms of skywave radio propagation (Ref. 6). The effects of the ionosphere on radio astronomy, which had its beginning around 1930, have also been of long standing interest. The advent of radio tracking of artificial satellites in 1957 added still another motivation for a more complete understanding and prediction of ionospheric phenomena. As an aside it is also of interest to note that ionization in the upper atmosphere is directly linked to solar activity and solar activity has been monitored in terms of Zurich sunspot number since 1755! Over the intervening 218 years a total of twenty consecutive eleven year sunspot cycles have been observed (Ref. 7).

In early 1970 it was decided by NASA-GSFC that this wealth of theoretical and experimental background should be applied toward the development of a worldwide ionospheric correction model consistent with anticipated tracking accuracy requirements of the 1973 and beyond time frame. The philosophy was to start with the promising closed form mathematical profile description first suggested by Kazantsev (Ref. 8) and later modified by Bent in 1967 (Ref. 9). This profile was then to be related to empirically determined electron density decay factors derived from analysis of many thousands of satellite and ground based soundings, and satellite electron density measurements. The data of interest was already available for a seven year time span and stored in a number of data center archives. The ready availability of suitable large scale high speed computers in 1970 gave assurance that such a goal involving large scale data analysis was indeed feasible. By mid 1971 the basic NASA-GSFC ionospheric model had been developed and an extensive testing and evaluation took place. Since integrated electron content is the scaling parameter for ionospheric corrections to all satellite tracking data, every means available was used to compare this model with measured integrated content. The latter measurements

included: Faraday rotation from ATS-1 and ATS-3, group-phase velocity measurements using NASA Explorer series spacecraft, two-frequency ranging to ATS-3, intercomparisons with the U. S. Army Map Service SECOR System, and ray tracing through composite profiles derived from bottom and topside sounding measurements. In other tests corrections were applied to numerous passes of previously uncorrected tracking data and postflight orbit computations were performed with the general result of a significant reduction in residuals. RMS observed minus calculated range, range rate or angle data were often reduced by factors of 4 or more. In addition many trajectory overlap tests were run which further indicated significant improvements in orbit computation accuracy. These tests included comparisons with existing but much cruder ionospheric correction models and here accuracy improvements by factors of two or more were observed (Ref. 10, 11). The final step was merging of the total NASA-GSFC ionospheric model with the Goddard Trajectory Determination System (GTDS) in time for successful operational support of the Radio Astronomy Explorer-B launched in June of 1973. The time scale from the initial concept of this project to final implementation was approximately 3 years. As implied in the initial comments, this work necessarily reflects an extension and application of the efforts of many researchers. However this particular NASA contribution is directly associated with those persons cited in Figure 1 and in particular with Dr. R. B. Bent and Ms. S. K. Llewellyn who were the principal persons involved in the analysis and formulations which led to the present NASA-GSFC ionospheric model. This work represents a part of the ongoing applied atmospheric physics effort (Figure 2) in the Geodynamics Program Division as directed toward such areas as high precision satellite radio tracking and satellite altimetry in support of such programs as the NASA-GSFC Earth and Ocean Physics Applications Program.

2.0 DEVELOPMENT OF THE NASA-GSFC IONOSPHERIC MODEL

2.1 DEVELOPMENT OVERVIEW

The types and quantity of measured data involved in the development of the NASA-GSFC ionospheric model are indicated in Figure 3. The starting point for the f_oF_2 and M(3000) F_2 worldwide time dependent spherical harmonic mapping was already available as a result of many years of research at the former National Bureau of Standards, Boulder, Colorado, now the National Oceanic and Atmospheric Administration - Boulder (Ref. 3 and Ref. 12 through 19).

As will be explained, f_oF_2 is the vertical sounding frequency related to the ionosphere profile maximum electron density. The M(3000) F_2 scalar factor (Figure 3) is the ratio of the MUF(3000) F_2 to f_oF_2 frequencies. The MUF (3000) F_2 is the highest frequency for a 3000 km single hop Earth point-to-point

GEODYNAMICS PROGRAM DIVISION
IONOSPHERIC MODEL
1970-1973

- PRINCIPAL SCIENTIST - DR. R. B. BENT*
- SUPPORTING STAFF - S. K. LLEWELLYN*
  G. NESTERCZUK*
  DR. S. RANGASWAMY**
- NASA-GSFC TECHNICAL OFFICER -
  P. E. SCHMID***
- NASA-GSFC RADIO WAVE PROPAGATION
  CONSULTANT - DR. J. W. MARINI***

* ATLANTIC SCIENCE CORPORATION
** OLD DOMININION SYSTEMS, INC.
*** NASA-GSFC

Figure 1

NASA-GSFC GEODYNAMICS PROGRAM DIVISION
ATMOSPHERE MODELING AND MEASUREMENT

IONOSPHERE

MODEL FOR TRAJECTORY COMPUTATION PROGRAMS

- HORIZONTAL GRADIENTS
- UPPER IONOSPHERE REALISTIC DECAY
- SCALE HEIGHT BASED ON ATMOSPHERIC PHYSICS
- SOLAR FLUX UPDATE

MEASUREMENT TECHNIQUES

- FARADAY ROTATION
- TRACKING SYSTEM RANGE AND RANGE RATE COMPARISONS
- TWO FREQUENCY RANGING
- SATELLITE DRAG EFFECTS

TROPOSPHERE

MODEL FOR TRAJECTORY COMPUTATION PROGRAMS

- SINGLE COMPUTATIONAL ALGORITHM FOR ALL ELEVATION ANGLES
- RADIO AND LASER

MEASUREMENT TECHNIQUES

- DRY-WET BULB TEMPERATURES,
- TOTAL PRESSURE
- RADIOMETER

Figure 2

NASA-GSFC IONOSPHERE MODEL DEVELOPMENT

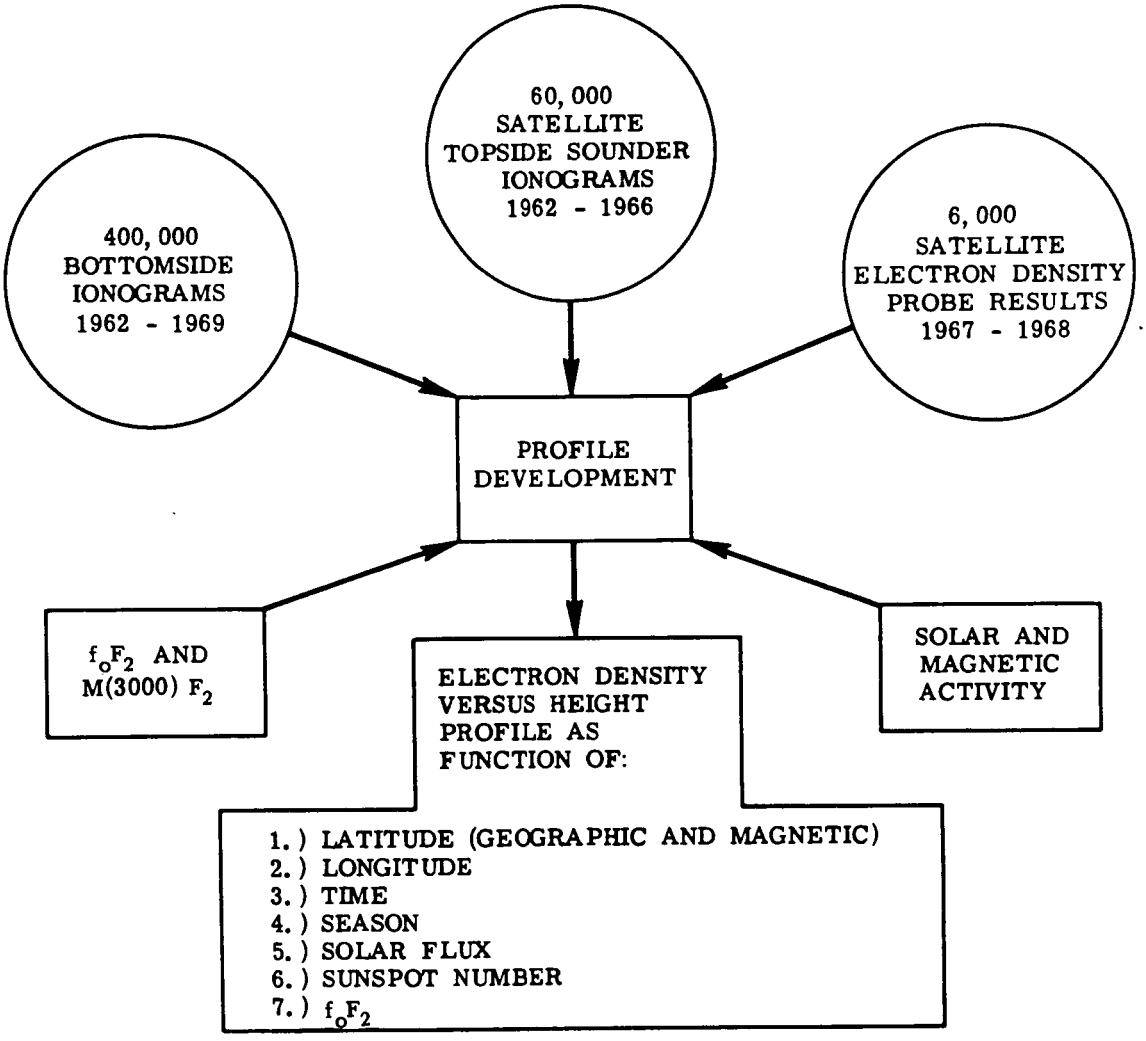

Figure 3

radio communication via the F_2 layer and is associated in this model with the height of the maximum electron density.

Finally the world map of critical frequency f_oF_2 which is directly related to maximum electron density is updated with predicted (or measured if available) solar flux activity on a daily basis from, for example, the National Space Science Data Center at NASA-GSFC. The basic coefficients of the spherical harmonic expansion of the world map are stored in the computer memory and called up as required. The values computed from these basic stored coefficients are then updated as a function of measured or predicted solar activity. Figure 4 indicates this overall basic implementation.

2.2 MODEL PARAMETERS

The mathematically closed form ionospheric profile is shown in Figure 5. It consists of segments of parabolic, parabolic-squared and exponential functions. The functions are matched in magnitude and slope at each boundary. The maximum electron density, N_m, as will be shown, is related to the $f_o F_2$ frequency. This density is on the order of 10^{11} to 10^{12} electrons per meter^3 depending on time of year, time of day, solar activity, geographic latitude and longitude and so on. The corresponding vertical total integrated electron content varies from 10^{16} to 10^{18} electrons per meter^2. Also the height of the maximum density, h_m, is a function of the scalar factor M(3000) F_2 and will typically range from 200 to 400 km. The parameters affecting profile shape (e.g. K_1, K_2, K_3, Y_m, Y_t) were empirically derived from the large data base indicated in Figure 3 and are stored in the computer in the form of look up values which are functions of latitude, longitude, $f_o F_2$ and time of year.

At this point a few brief comments regarding the nomenclature, origin and meaning of $f_o F_2$ and M(3000) F_2 is appropriate. It is well known by the communications engineer working with radio frequencies below 30 MHz that radio signals are reflected by apparently discrete ionospheric layers commonly termed E, sporadic-E, F_1, F_2 and so on. The daytime D layer is primarily an absorption layer (Ref. 20) that for example prevents broadcast signals (500 to 1600 kHz) from "Skipping out" to distant points during daylight hours. The profile in Figure 5 obviously does not model these discrete layers; however, the maximum density corresponds to the most important reflecting layer, namely the F_2 region. Since satellite tracking biases result from integrated effects through the entire ionosphere the lower ionosphere fine structure can be generally ignored. The origin of the nomenclature D, E, or F layer is worth mentioning as a matter of historical interest. In the early experimental work of Sir Edward Appleton his first ionospheric reflections were obtained from an apparent layer which he

NASA-GSFC IONOSPHERE MODEL IMPLEMENTATION

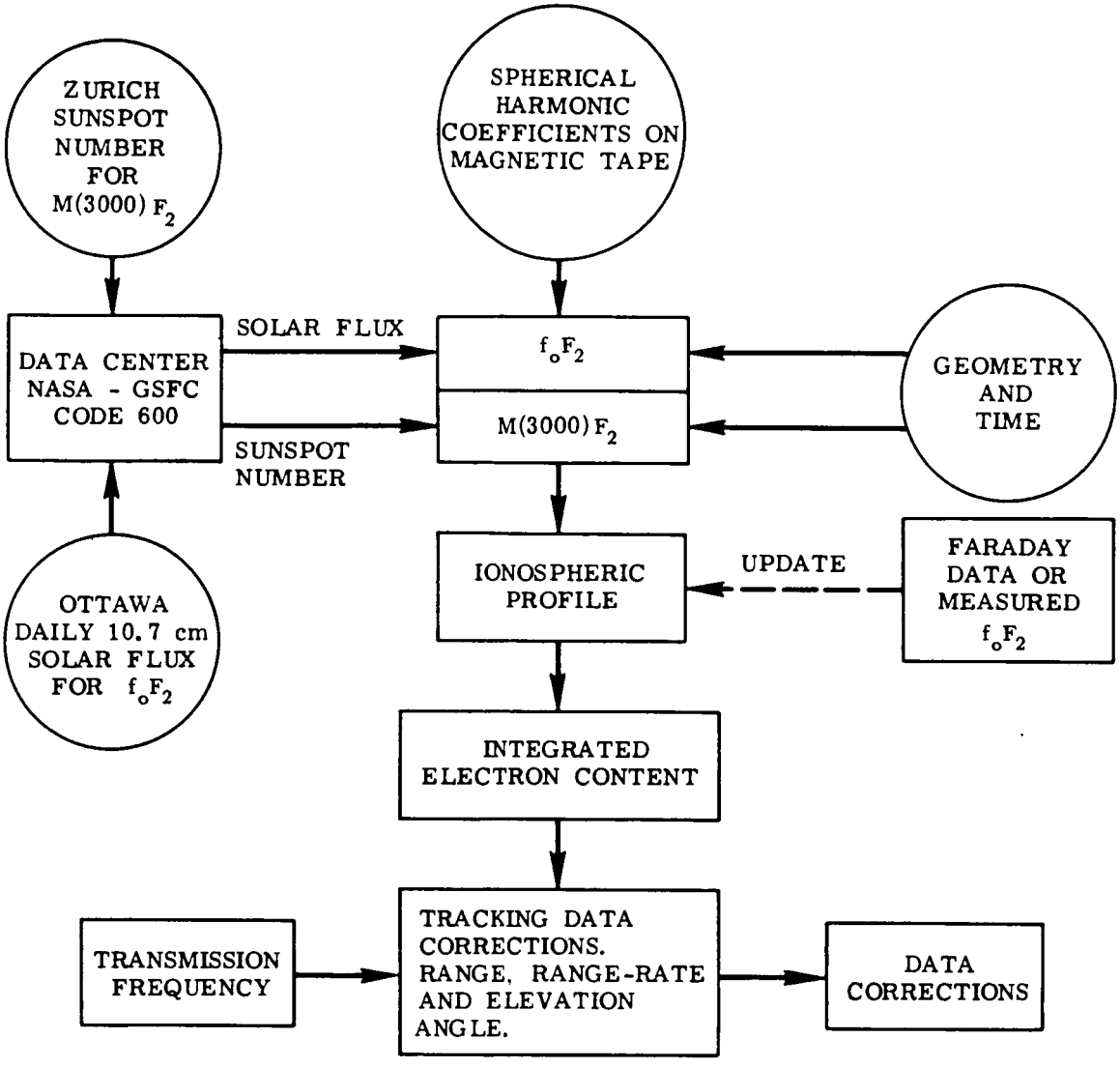

Figure 4

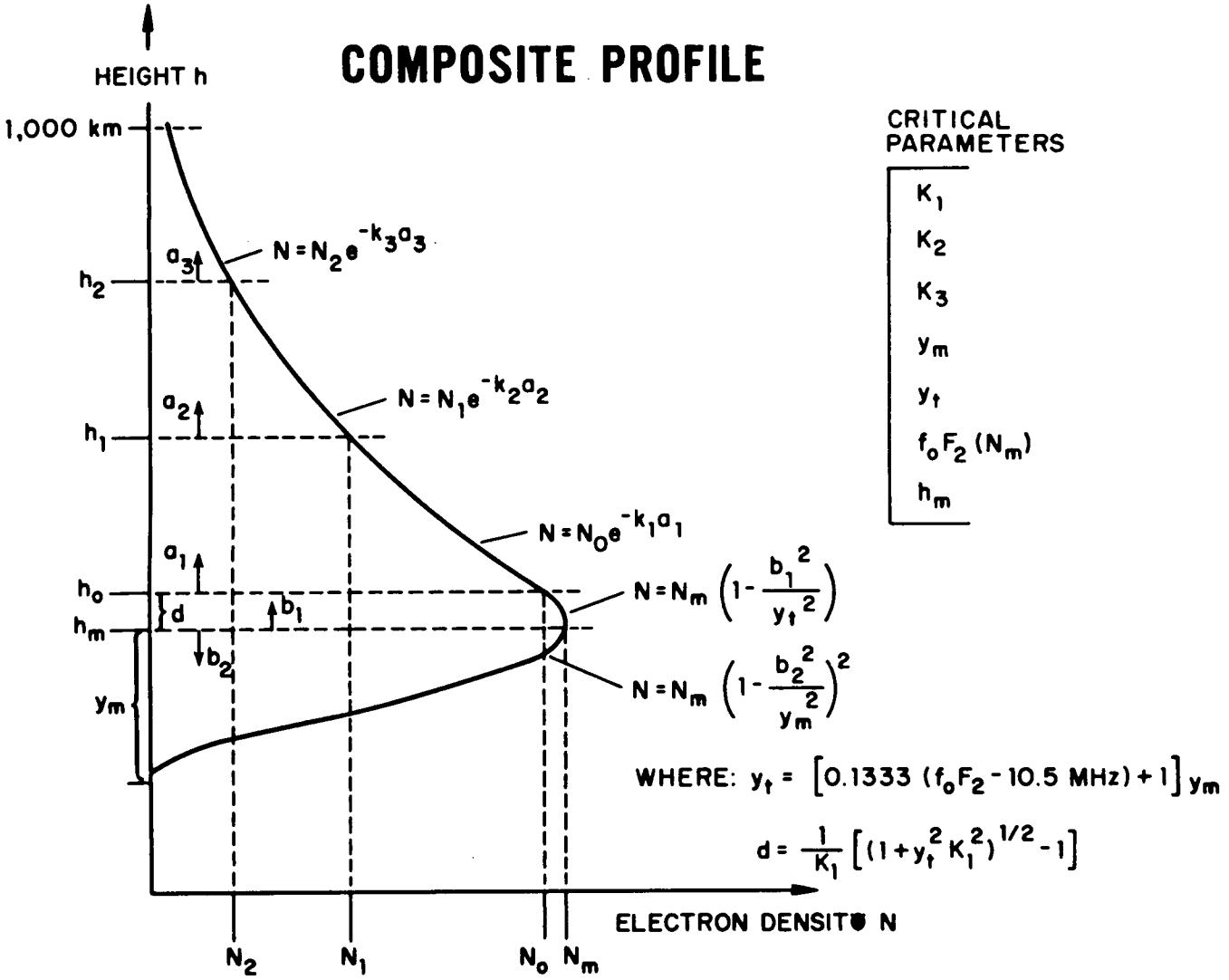
COMPOSITE PROFILE
HEIGHT h
1,000 km
h_2
h_1
h_o
h_m
a_3
a_2
a_1
d
b_1
b_2
y_m
$N = N_2 e^{-k_3 a_3}$
$N = N_1 e^{-k_2 a_2}$
$N = N_o e^{-k_1 a_1}$
$N = N_m \left(1 - \frac{b_1^2}{y_t^2}\right)$
$N = N_m \left(1 - \frac{b_2^2}{y_m^2}\right)^2$
N_2
N_1
N_o
N_m
ELECTRON DENSITY N
CRITICAL PARAMETERS
K_1
K_2
K_3
y_m
y_t
$f_o F_2 (N_m)$
h_m
WHERE: $y_t = \left[0.1333 (f_o F_2 - 10.5 \text{ MHz}) + 1\right] y_m$
$d = \frac{1}{K_1}\left[(1 + y_t^2 K_1^2)^{1/2} - 1\right]$

Figure 5

simply called the E layer corresponding to the notation of the reflected $\vec{E}$ vector of the electromagnetic radiation. Later in the winter of 1925 he obtained reflections from two other layers below and above the E layer height and termed them respectively D and F. He reasoned there might be still additional layers both above and below the originally discovered E layer and hence retained this nomenclature rather then renaming the layers, for example A, B, C and so on (Ref. 21). Later the daytime F layer was found to split into two layers which are now commonly termed F_1 and F_2. The F_2 layer corresponds to the layer of maximum ionospheric electron density. The f_xF_2 frequency, or often termed MUF (ZERO) F_2, is the highest vertical sounding frequency which will be returned to Earth. The relationship between $f_o F_2$ and $f_x F_2$ is described in section 2.3. The nomenclature is again traced to radio communications applications, where zero means vertical or zero skip distance and MUF is "maximum usuable frequency" for reflection. Similarily the MUF $(3000)F_2$ is the maximum usuable frequency for a communications single hop of 3000 km from the F_2 layer. The latter is directly related to the height, h_m, of the peak of the F_2 layer.

The computer stored modeled parameters thus fall into two categories. These are the profile shaping factors determined empirically and the factors which describe the worldwide maximum density and height of maximum density, primarily $f_o F_2$ and $M(3000)F_2$ as updated with either predicted or measured solar activity. Where: $M(3000)F_2 = MUF(3000)F_2 \div f_o F_2$.
Solar activity is obtained from two data bases – namely, Zurich sunspot number and solar flux as measured at the 10.7cm wavelength. The sunspot history, as indicated previously goes back to the year 1755, and is derived from an observer's numerical count of sunspots. The two data types have been shown to reflect the same information and one empirical relationship (Ref. 22) between the two is given by:

$$\phi = (63.75 + 0.728\,R + 0.00089\,R^2)\,10^{-22} \quad (1)$$

watts/meter^2/Hz

Where: ϕ = 10.7λ flux

R = average Zurich sunspot number

2.3 MAXIMUM ELECTRON DENSITY AND HEIGHT OF MAXIMUM DENSITY

The familiar Appleton - Hartree equation relating index of refraction in a charged particle plasma in the presence of a magnetic field is traced back to at least 1927 (Ref. 23). This equation has been applied to ionospheric phenomena in a variety of approximate forms and the approximation validity is largely dependent on the particular portion of the radio frequency spectrum of interest. For example, at frequencies of 140 MHz neglecting the effect of the Earth's magnetic field introduces a maximum error of 2% and this error decreases rapidly for higher frequencies. At typical vertical sounding frequencies ($f_o F_2$) ranging from 5 MHz to 15 MHz the absorption terms can be ignored for refraction calculations but the Earth's magnetic field must be included. Reflection for vertical sounding occurs whenever the index of refraction tends to zero and this can be calculated for a given density from the simplified Appleton - Hartree equation given below:

$$\mu^2 = 1 - \frac{X}{1 - \frac{1}{2} Y_T^2/(1-X) \pm \left[\frac{1}{4} Y_T^4/(1-X)^2 + Y_L^2\right]^{1/2}} \qquad (2)$$

Ionospheric index of refraction squared neglecting absorption

- c = free-space velocity of light
- e = charge on an electron
- f = $\omega/2\pi$ = frequency of a radio wave
- H = geomagnetic field intensity
- m = mass of an electron
- N = number density of free electrons
- ϵ_0 = electric permittivity of free space
- θ = angle between wave normal and geomagnetic field
- λ = $2\pi c/\omega$ = free-space wavelength of a radio wave
- μ = real part of the refractive index
- μ_0 = magnetic permittivity of free space
- ω = angular frequency of a radio wave
- ω_H = μ_0 He/m = angular gyro frequency of an electron
- ω_L = $\omega_H \cos\theta$
- ω_N = $\sqrt{Ne^2/\epsilon_0 m}$ = angular plasma frequency
- ω_T = $\omega_H \sin\theta$
- X = ω_N^2/ω^2
- Y = ω_H/ω
- Y_L = ω_L/ω
- Y_T = ω_T/ω

References: 23, 24

For purposes of calculating maximum electron density at the F_2 layer the conditions leading to $\mu^2 = 0$ in equation (2) must be examined at the $f_0 F_2$ frequency. The presence of the static geomagnetic field, makes the ionosphere anisotropic or doubly-refracting, for radio waves. A radio wave of general polarization, on entering the ionosphere, will be split up into two waves each having a characteristic polarization. The relative amplitudes of the waves will depend on the original polarization. Each wave will then travel with its own characteristic velocity and attenuation. The two waves will, in general, have elliptic polarizations in opposite senses and are termed the "ordinary" and "extra-ordinary" waves. Each wave is reflected at a level where its refractive index tends to zero in the absence of collisions. Hence each wave will have its own 'critical' or 'penetration' frequency which is the maximum frequency which can be reflected by the layer.

The index of refraction for the two waves is given by taking the sign before the square root in equation (2) as positive and negative for the ordinary and extra-ordinary respectively. The ordinary critical frequency f_0F_2 and the extra-ordinary critical frequency f_xF_2 are related by the formula

$$(f_0F_2)^2 = (f_xF_2)^2 - f_H(f_xF_2) \tag{3}$$

where f_H is the gyrofrequency of electrons.

$$f_H = \frac{e}{2\pi m} |\vec{B}| = 2.84 \times 10^{10} |\vec{B}| \; H_z$$

($\vec{B}$ in webers/meter^2)

when: $f_0F_2 >> f_H$

$f_xF_2 >> f_H$

we can rewrite equation 3 as:

$$f_x F_2 - f_0 F_2 \cong \frac{1}{2} f_H \tag{4}$$

For calculating maximum electron density $f_o F_2$ is usually used since it is most easily measured. For calculating skip communications via the F_2 layer $f_x F_2$ is usually mapped, using equation 4 to obtain $f_x F_2$ from measured $f_o F_2$ (Ref. 17). Figure 6 is a world map of the gyro frequency which can be used to convert between the $f_o F_2$ and $f_x F_2$ frequencies.

The expression for maximum electron density is obtained from equation 2 at the ordinary critical frequency (i.e. $f_0 F_2$) as:

$$N_{max} = \frac{(f_0 F_2)^2}{80.6} \text{ electrons/meter}^3 \tag{5}$$

(where $f_0 F_2$ is in Hz)

The height of the maximum density is calculated on the basis of the equations of Appleton and Beynon (Ref. 25). The required $M(3000)F_2$ or M factor (also see section 2.2) predictions are obtained from a generalized data set issued by the National Oceanic and Atmospheric Administration. The equation used for the height of maximum electron density in the NASA-GSFC model is given by:

$$h_m = 1346.92 - 526.40M + 59.825M^2 \quad \text{km}$$

where

$$M = \frac{MUF(3000)\, F_2}{f_0 F_2} \tag{6}$$

WORLD MAP OF GYRO FREQUENCY (MHz)

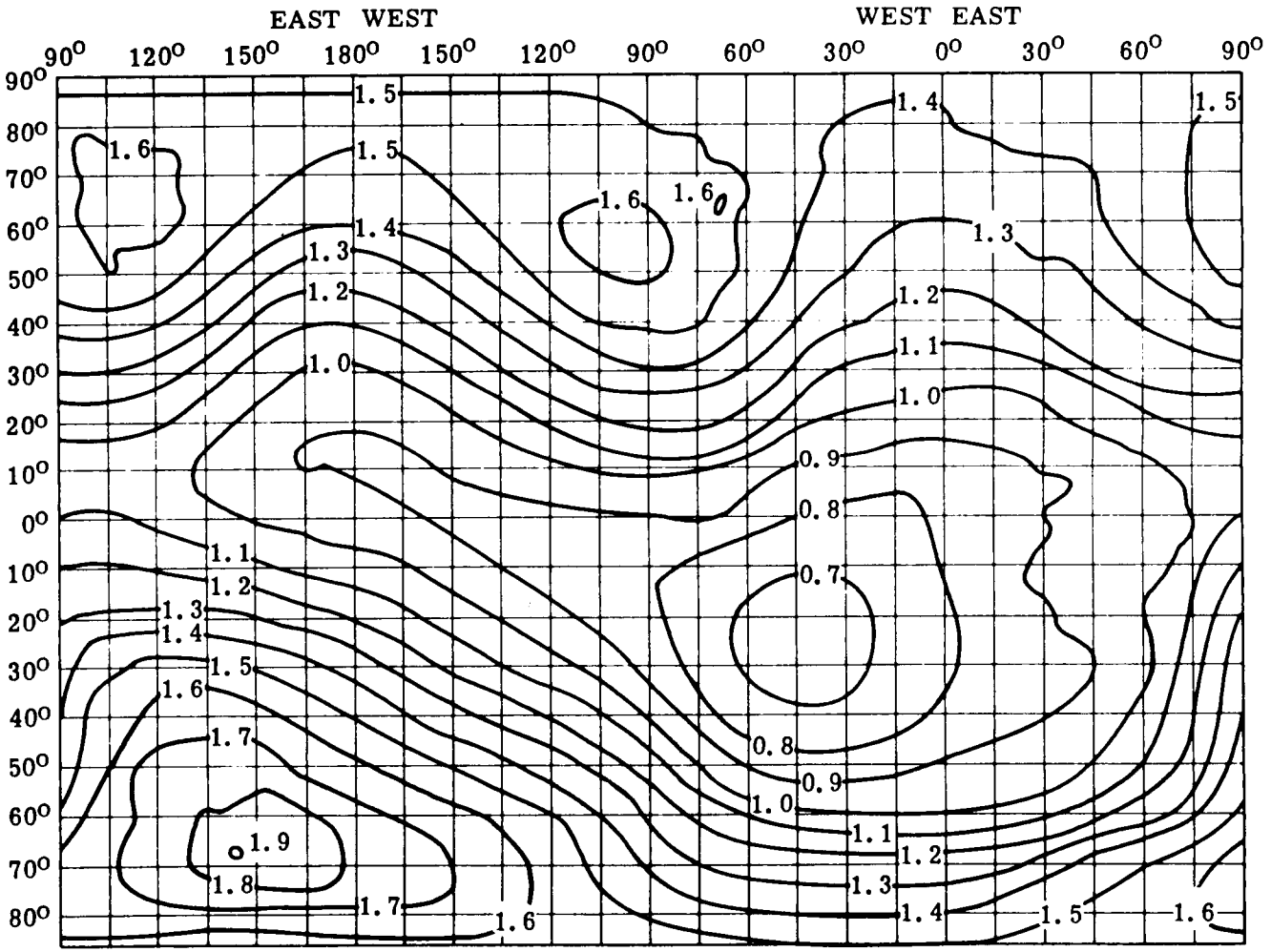

Figure 6

2.4 SPHERICAL HARMONIC MAPPING OF f_oF_2 AND M(3000)F_2

As indicated in Figure 4 a basic unchanging set of harmonic coefficients are stored in the computer for both f_oF_2 and M(3000)F . These coefficients reflect both a time and geographical dependence. The $f_0 F_2$ set is scaled by a quadratic function of solar flux. The M(3000)F_2 is scaled by a linear function of sunspot number. The choice of update parameters is a matter of historical development and the entire update information can in fact be tied to solar flux measurements if deemed desirable. In addition, as a result of the analysis of the 400,000 world-wide bottomside ionograms, a latitude dependent bias in $f_0 F_2$ was discovered relative to previously presented data by the National Oceanic and Atmospheric Administration (NOAA-Boulder, Colorado). Thus this modelling effort which for f_oF_2 and M(3000)F depended heavily on the earlier work at Boulder (Ref. 12 to 19), has provided a marked refinement for those geographical regions significantly remote from the U. S.

For both the $f_0 F_2$ and M(3000)F_2 the form of the basic harmonic expansion is:

$$\Omega(\phi, \lambda, T) = \sum_{k=0}^{K} D_k(T)\, G_k(\phi, \lambda) \tag{7}$$

where: ϕ (Geographic Latitude)
λ (Longitude)
T (Time) = local mean hour angle $-180° < T < 180°$

The time dependent Fourier Series modulating the geographical term models the diurnal and seasonal variations and has the form:

$$D_k(T) = A_0^{(k)} + \sum_{j=1}^{H} \left(A_j^{(k)} \cos_j T + B_j^{(k)} \sin_j T\right) \tag{8}$$

where
$H = 6$ for f_oF_2
$H = 4$ for M(3000)F_2

The latitude and longitude spherical harmonic terms are expanded as associated Legendre functions much in the same manner as the geopotential function used in all orbit computation.

The number of terms used in this harmonic representation is given in Table 1. The number of terms selected takes into account the maximum number warranted in light of the data base quality to which these functions have been fitted.

Table 1
Harmonic Coefficients

Number of Terms			
	Time Series	Geographic Terms	Total
$f_0 F_2$	13	76	988
$M(3000)F_2$	9	49	441

Figure 7 presents the type of map resulting from such a representation. This particular example is an $f_x F_2$ monthly mean prediction for August 1963 at UT 0600 hours. With the present NASA capability, daily updates for $f_o F_2$ and $M(3000)F_2$ can be made and this was actually done for the critical first few days following the June 1973 launch of the Radio Astronomy Explorer-B.

2.5 INDEX OF REFRACTION FOR FREQUENCIES ABOVE 100 MHz

The satellite tracking data acquired at frequencies above 100 MHz will be biased while traversing the ionosphere because the index of refraction is other than that of free space (i.e. $\mu = 1.0$). Equation 2 for frequencies above 100 MHz can then be approximated by:

$$\mu \doteq \left(1 - \frac{N_e e^2}{\epsilon_o m \omega^2}\right)^{1/2} \doteq \left(1 - \frac{40.3 N_e}{f^2}\right) \qquad (9)$$

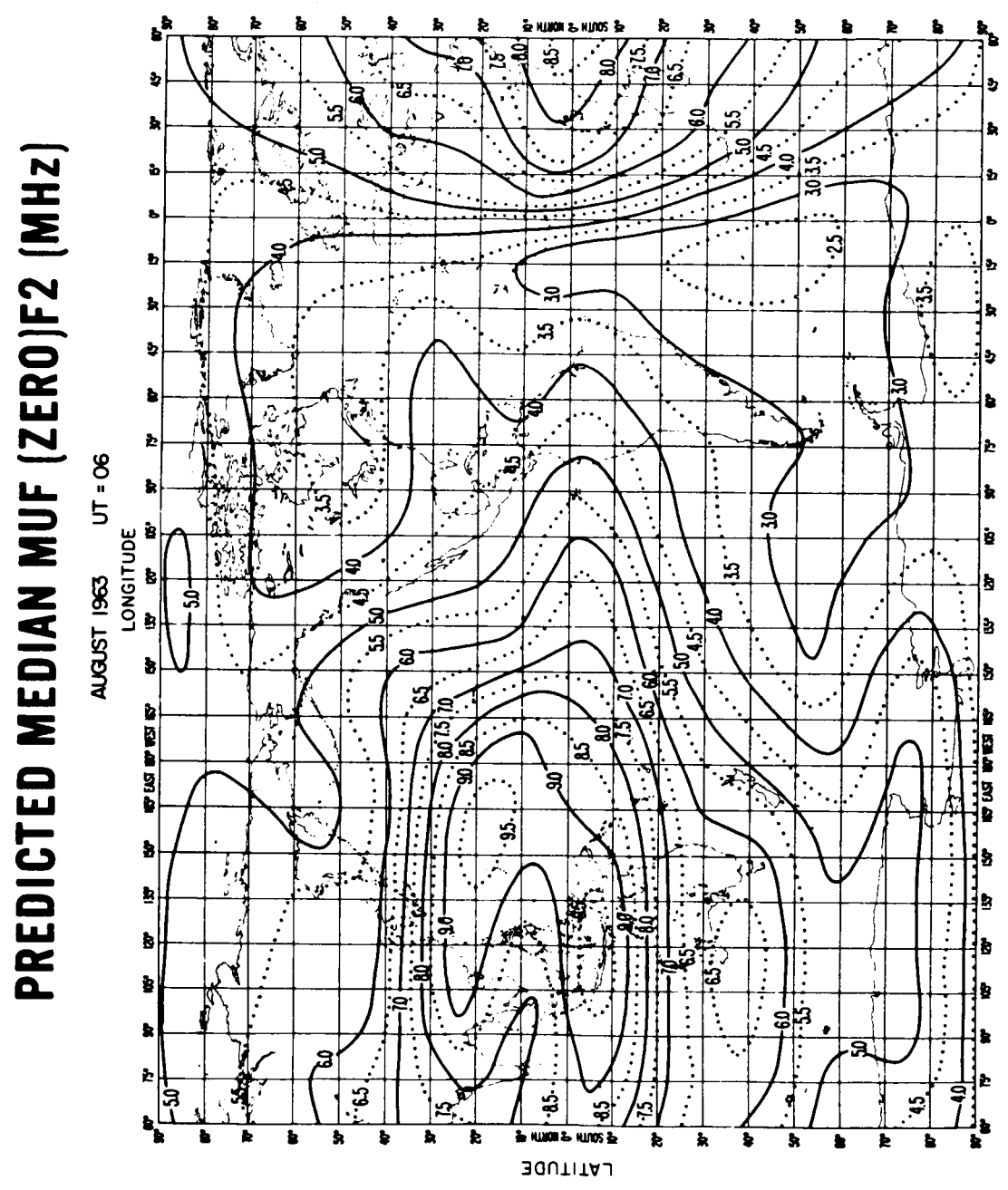
PREDICTED MEDIAN MUF (ZERO)F2 (MHz)
AUGUST 1963 UT = 06
LONGITUDE
LATITUDE

Figure 7

where: N_e = Electron density (electrons/meter^3)
e = Electron charge = 1.602×10^{-19} coulombs
m = Electron mass = 9.11×10^{-31} kilograms
ϵ_0 = Free space dielectric constant
= 8.855×10^{-12} farads/meter
ω = $2\pi f$ (radians/sec)

The tracking data distortion experienced relative to free space, is related to the integral of the electron density along the ray path. In all cases the systematic distortion will be scaled by the integrated content (electrons/meter^2) along the ray path, however the exact manner in which the radio measurements are affected will depend on the details of the tracking system involved.

2.6 INTEGRATED ELECTRON CONTENT PREDICTION

The profile shown previously in Figure 5 is easily integrated in closed form and thus permits calculation of predicted total vertical integrated content over any geographical region. In satellite data corrections however the total integrated content of interest is that along the path between tracking station and satellite. It has been found that a good estimate of the total path delay can be established by using the vertical integrated content divided by the sine of the local elevation angle, E*, at the point the ray path intercepts the maximum electron density. The geometry involved is straightforward and with reference to Figure 8, is as follows:

$$E^* = \arccos\left[\frac{a}{a + h_m} \cos E\right] \tag{10}$$

where: a = Earth radius
h_m = height of maximum electron density
E = elevation angle at tracking station
E^* = local elevation angle at h_m

Since Doppler bias results from the time variation of the index of refraction another parameter used is the elevation angle rate at the height of the maximum which is given by:

$$\dot{E}^* = \left\{\frac{a\,\dot{E} \sin E}{a + h_m}\right\} \left\{\frac{1}{\left[1 - \left(\frac{a}{a + h}\right)^2 \cos^2 E\right]^{1/2}}\right\} \tag{11}$$

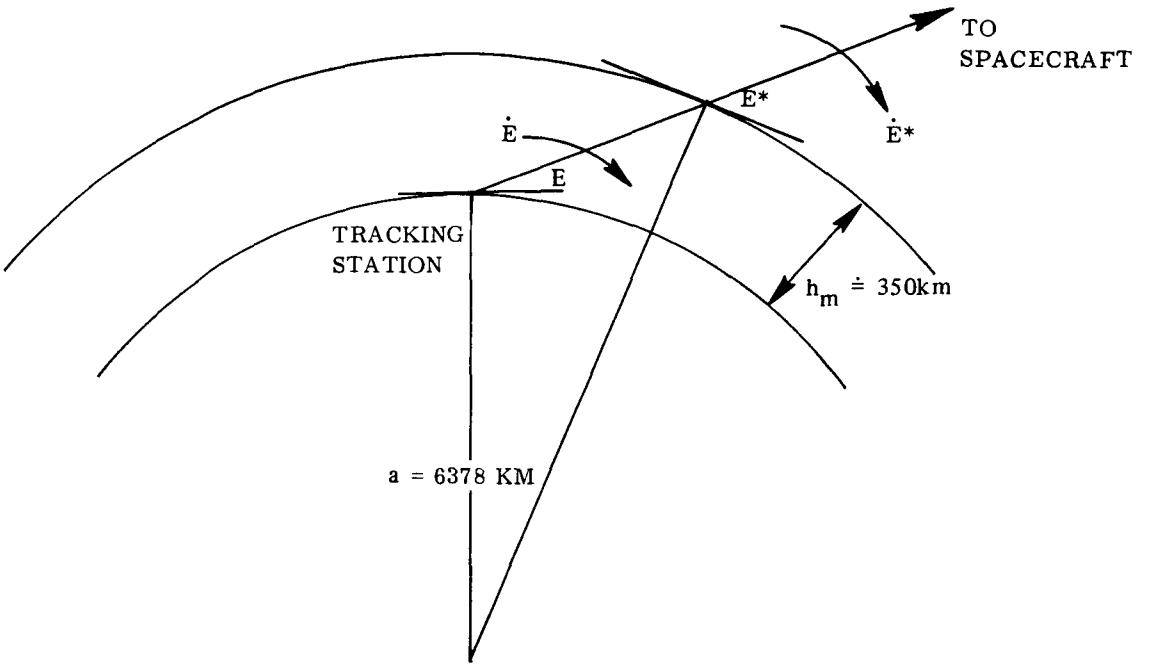

Figure 8

where: $\dot{E}$ = elevation angle rate as observed at tracking station
$\dot{E}^*$ = elevation angle rate at h_m

The NASA model thus computes the intercept of the tracking station to satellite ray path with the maximum density layer in the ionosphere for any station location on Earth and provides the appropriate integrated electron content which is in turn used in all subsequent tracking data correction equations.

3.0 IONOSPHERE MODEL VERIFICATION AND IMPLEMENTATION

3.1 TRACKING DATA CORRECTION EQUATIONS

As indicated earlier, the exact form of the ionosphere tracking data correction equations is a function of the specific tracking systems employed. However, certain simplifications are possible in order to gain insight into the problem. The results derived in the following are in fact applicable to NASA range and range-rate tracking as a consequence of the manner in which phase and frequency

relationships are maintained throughout the satellite tracking link. The following will indicate mathematically how range and range rate biases are introduced and the results will be shown to be consistent with the often presented formulation for range bias:

$$\Delta R = \frac{40.3}{f^2} \int N_e \, dR \text{ meters} \tag{12}$$

f = frequency in Hz
N_e = electron density along ray path electrons/meter^3

integral taken along ray path between tracking station and satellite

In the model described:

$$\int N_e \, dR = \frac{I_v}{\sin E^*} \text{ electrons/meter}^2 \tag{13}$$

(where I_v is verticle electron content calculated at ray path intercept with region of maximum electron density)

All NASA range and range rate systems employ narrowband phase modulated CW systems having the form:

$$E = A \cos (\omega_c t + \beta \sin \omega_m t) \tag{14}$$

$\omega_c = 2\pi f_c$ = carrier angular frequency
$\omega_m = 2\pi f_m$ = modulation angular frequency
β = modulation index

The modulation index, β, is typically maintained between 0.5 and 1.5 radians. The NASA tracking systems employ transmission from ground station to a spacecraft transponder which in turn retransmits a radio signal to the ground station (e.g. Ref. 26). Thus the ionosphere is traversed twice and two frequencies are involved since the transponded frequency is offset from the spacecraft received frequency. The two frequency effect can in general be considered by using:

$$\frac{1}{f^2} = \frac{1}{2}\left(\frac{1}{f_{up}^2} + \frac{1}{f_{down}^2}\right) \tag{15}$$

However the precise formulation for the effective frequency, f, must be made in light of the specific tracking system considered (Ref. 27).

For illustrative purposes the frequency translation can be ignored and the radio signal demodulated as if the ionosphere were traversed twice by a coherently transponded carrier signal at frequency, f_o.

The narrowband phase modulated signal can be considered to consist of 3 principal frequencies – namely, a carrier and two symmetrically situated sidebands (Ref. 28). The form of such a signal with amplitudes normalized for simplicity is:

$$E = \cos \omega_o t + \cos (\omega_o + \omega_m) t - \cos (\omega_o - \omega_m) t \tag{16}$$

As seen by equation 8 the index of refraction is frequency dependent and the effect on the range measurement and coherent Doppler phase can be calculated with reference to Figure 9. The functional representation includes a phase detector for range measurement determination and a Doppler extractor for range rate determination. In principal the demodulation requires the multiplication of signals by means of a non-linear device and undesired higher order terms are filtered out. Anyone familiar with the actual mechanization of a system such as the Goddard Range and Range Rate System will realize the gross oversimplification depicted by Figure 9. However the mathematics of the more complex system can be shown to reduce to an equivalent coherent spacecraft turnaround with a unity transponder frequency translation ratio (Ref. 26). Referring back to Figure 9, when the indicated multiplications are performed and the desired signals extracted one obtains:

$$\phi_R = \frac{-2\omega_m R}{c} - \frac{40.3\,\omega_m}{c f_o^2} \int N_e \, dR \qquad \text{Radians} \tag{17}$$

(Range Tone Phase)

EFFECT OF IONOSPHERE ON NARROW BAND
PHASE MODULATED SIGNALS

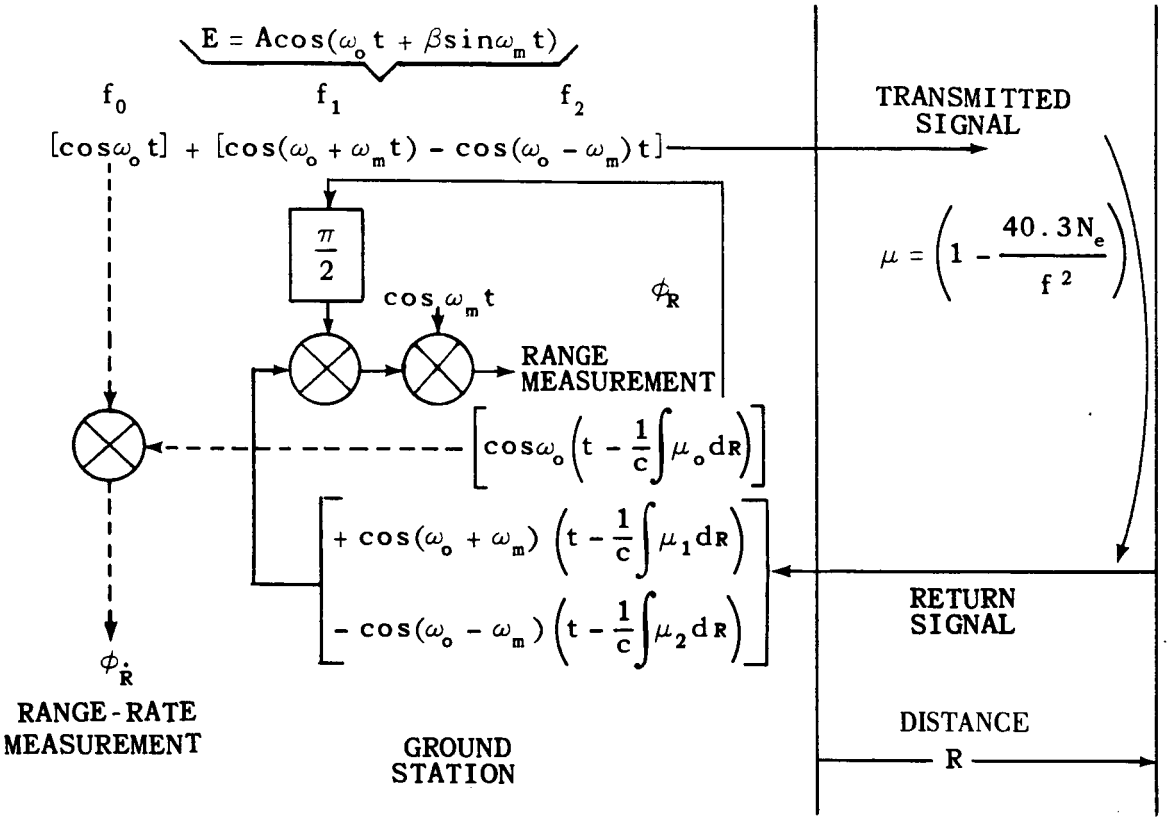

Figure 9

and

$$\dot{\phi}_R = \frac{-2\omega_o R}{c} + \frac{40.3\,\omega_o}{c f_o^2} \int N_e\, dR \quad \text{Radians} \tag{18}$$

(Carrier Phase)

and the two-way integrated electron content is modeled as:

$$2\int_0^R N_e\, dR = \frac{2I_v}{\sin E^*}$$

It should be pointed out that equations 17 and 18 are again approximations (for example Ref. 29) which neglect higher order terms. However the error introduced is negligible at the frequencies considered being less than 0.3% in the worst case.

The interesting fact to note with regard to the ionospheric effect in equations 17 and 18 is that whereas the range tone measurement experiences a phase delay the carrier phase measurement undergoes an effective phase advance. The range tone delay is used as a measure of the range to the spacecraft. The carrier phase shift is differenced over a short time span (typically 0.5 seconds) to provide an average Doppler frequency which is directly proportional to range rate. It is apparent that the effect of the ionosphere on the two types of measurements is of opposite sign and hence should in principle allow one to solve for integrated electron content by comparing range differences with integrated Doppler and/or differentiated range measurements directly with range rate measurements. Such comparisons have in fact been made and used as one means of evaluating the NASA-GSFC Ionospheric model. The difficult task has been selection of appropriate data smoothing, editing, and compression techniques. This is because the inherently coarser range tone (typically 20 kHz at VHF) phase measurement is to be compared with the high resolution carrier phase data which can, with 5 second averaging, measure range rate to a resolution of 0.5 cm/sec at 140 MHz and to better than 0.1 cm/sec at 2 GHz (Ref. 1).

While angle data from antenna pointing is also available from range and range-rate sites it is seldom used in NASA orbit computation simply because the data quality is not consistent with the high accuracy range and range-rate measurements. Often range-rate only or range only orbit solutions are performed depending on satellite geometry and distance of spacecraft from the tracking site.

The NASA 136 MHz Minitrack interferometer measures direction cosines and for this system ionospheric corrections are applied in terms of angle of arrival. Unfortunately no simple formulation exists to relate this ionospheric correction. It will suffice to say that the ionospheric ray bending (in contrast to tropospheric effects) is predominant at 136 MHz and this is discussed in reference 30. The formulation adopted for the Goddard Trajectory Determination System to calculate angular deviations is presented in Ref. 31. Ionospheric effects in satellite-to-satellite tracking are discussed in reference 32.

3.2 GROUP-PHASE PHENOMENA

The results presented as equations 17 and 18 can also be arrived at considering group and phase velocity effects through a dispersive media. Using such an approach leads to the conclusion that these equations also apply, again to a certain approximation, to pulse systems and amplitude modulated systems. It is beyond the scope of this report to present a detailed discussion of such concepts as group velocity and phase velocity. However further discussion is presented in Ref. 3, 33, and 34.

The important consideration herein is experimental. That is, the observability of such phenomena as predicted by equations 17 and 18.

Figure 10 is obtained from a comparison of range and range-rate data and depicts extraction of the ionosphere induced range rate bias while using the NASA-GSFC 136-148 MHz range and range-rate tracking system. As the elevation angle scan rate tends to zero (at the relative time of 150 seconds) the range rate bias also tends to zero. This is the result predicted by the time derivative of equation 18 if all changes in total electron content along the propagation path can be attributed to the elevation angle scan. This is a reasonable assumption for near Earth spacecraft, however for deep space corrections, where the maximum scan rate is essentially Earth rotation of 7.3×10^{-5} radians/sec, the time rate of electron content change due to diurnal effects must also be included.

Figure 11 shows the group-phase comparison for a 500 second data stretch where data was recorded at a 4 per second rate. The data compression utilizing polynomial smoothing compressed the data over 10 separate sub-arcs and the

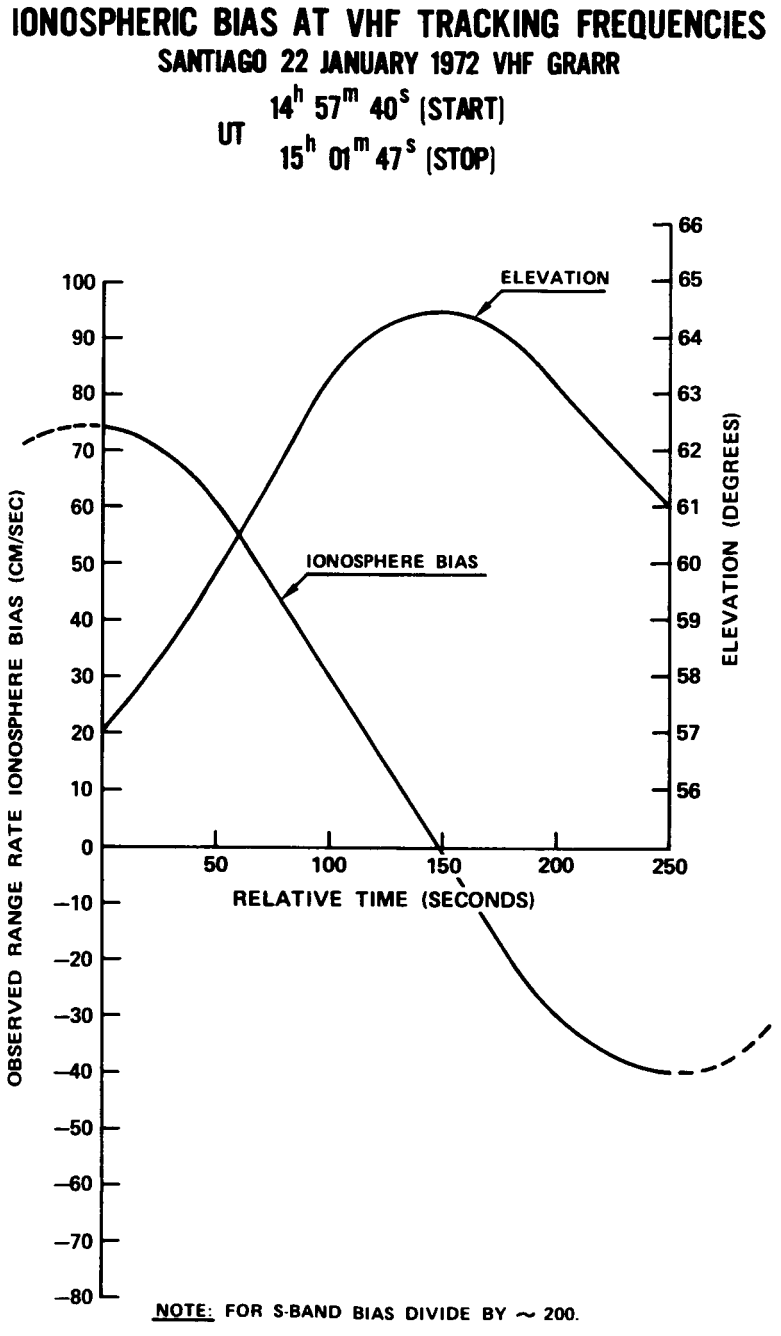
IONOSPHERIC BIAS AT VHF TRACKING FREQUENCIES
SANTIAGO 22 JANUARY 1972 VHF GRARR
UT 14h 57m 40s (START)
15h 01m 47s (STOP)
ELEVATION
IONOSPHERE BIAS
OBSERVED RANGE RATE IONOSPHERE BIAS (CM/SEC)
ELEVATION (DEGREES)
RELATIVE TIME (SECONDS)
100
90
80
70
60
50
40
30
20
10
0
−10
−20
−30
−40
−50
−60
−70
−80
66
65
64
63
62
61
60
59
58
57
56
50
100
150
200
250
NOTE: FOR S-BAND BIAS DIVIDE BY ~ 200.

Figure 10

VHF GRARR IONOSPHERE GROUP/PHASE MEASUREMENT

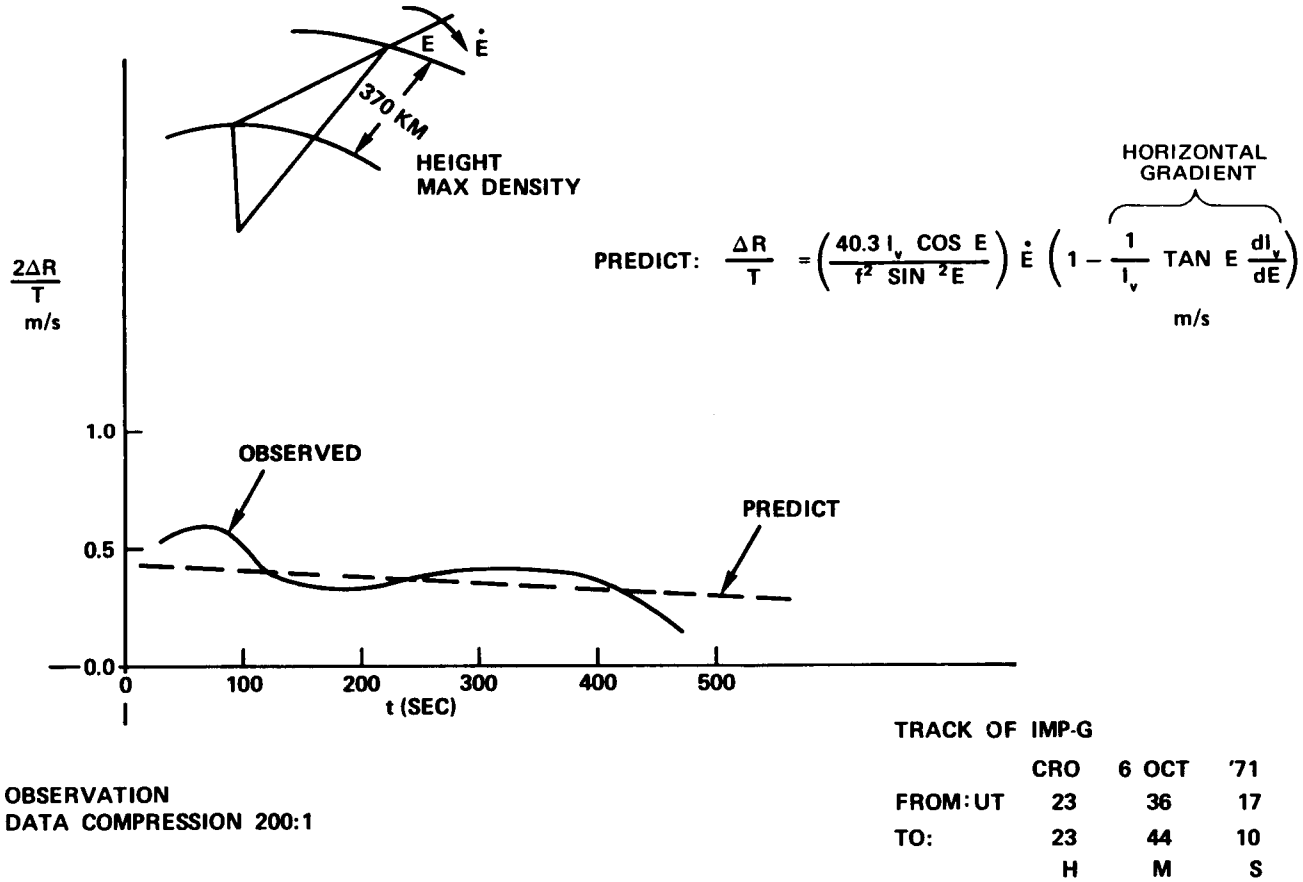

Figure 11

resultant curve is termed "observed". Experience based on both simulated and observed data indicates that near Earth polynomial smoothing of data must be applied with caution to prevent errors introduced by the smoothing process itself (e.g. Ref. 35). The VHF range-rate data has been noted to be consistently of higher quality than range data in the sense that compressed range rate values time tagged at the same instant are generally independent of the degree of fit once polynomials over a cubic are employed and data stretches are limited to 50 seconds or less. Range data on the otherhand is to a certain extent sensitive to degree of fit and the modulation of "observed" values in Figure 9 is attributed to low frequency cyclic noise on the range data. This range noise appears to be a function of spacecraft spin and range tracking loop performance under high dynamics (i.e. perigee passes of near Earth satellites). However it must be mentioned that the measurements being performed are far beyond the initial design intent for tracking system performance. In fact if range data could be processed to achieve the same accuracy for range rate estimates as the carrier determined range-rate there would be no further need for range-rate measurements.

Figure 11 also indicates the importance of considering horizontal electron density gradients in modeling of the ionosphere for the purpose of correcting tracking data bias. In this particular example the predicted gradient shown in Figure 12 accounts for approximately 20% of the predicted range rate bias shown in Figure 11. The effect of horizontal gradients is further demonstrated by Figure 13. In this case a typical simulated satellite overhead pass is considered and the range bias at 140 MHz compared for polar and equatorial passes. The difference between the two results again indicates the importance of modeling horizontal gradients.

3.3 TWO-FREQUENCY RANGING

Another well established means for experimentally determining integrated electron content is to perform satellite range measurements at two widely separated frequencies and comparing the results in view of the $1/f^2$ dependence of ionospheric group delay. When one undertakes such measurements the practical problems of calibration, data extrapolation, time tagging and data compression become a primary concern. As usual, relative measurements are rather straightforward and absolute measurements become increasingly difficult as higher accuracy is sought.

An example of two frequency ranging is shown in Figure 14 where measurements were made at C-Band (4-6 GHz Applications Technology Satellite Ranging System) and at VHF (140 MHz). The tracking was between Rosman, N. C. and

EXAMPLE OF PREDICTED IONOSPHERE GRADIENT DURING SATELLITE TRACK

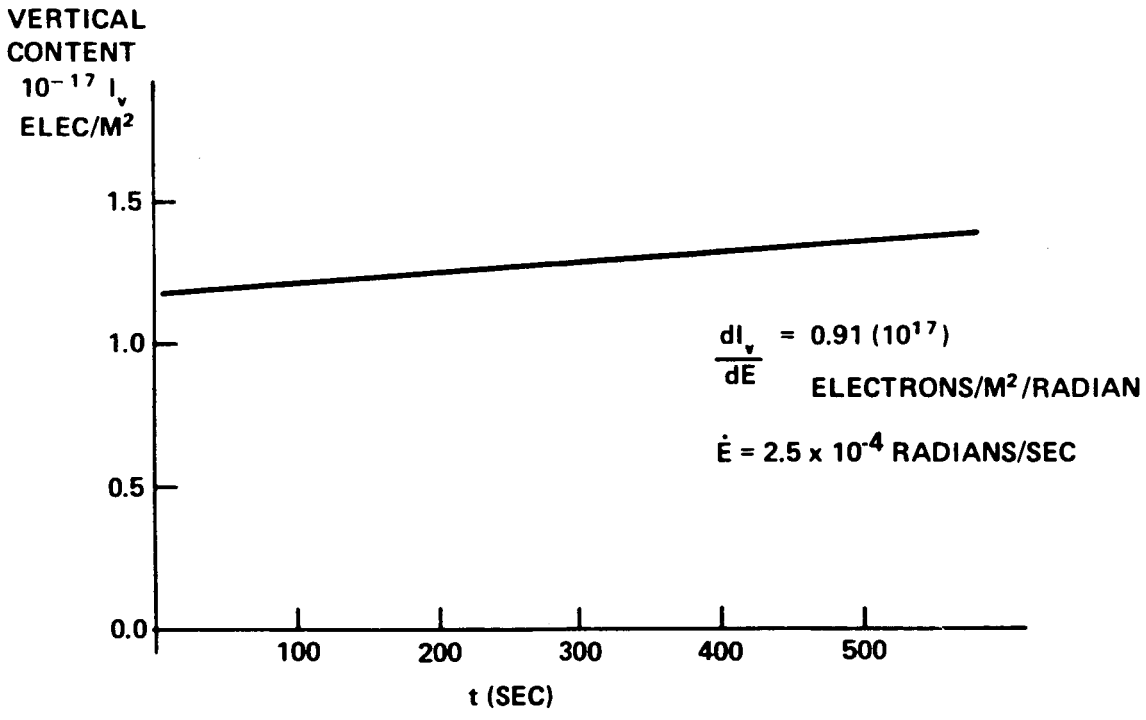

Figure 12

EXAMPLE OF IONOSPHERIC MODEL AZIMUTH DEPENDENCE

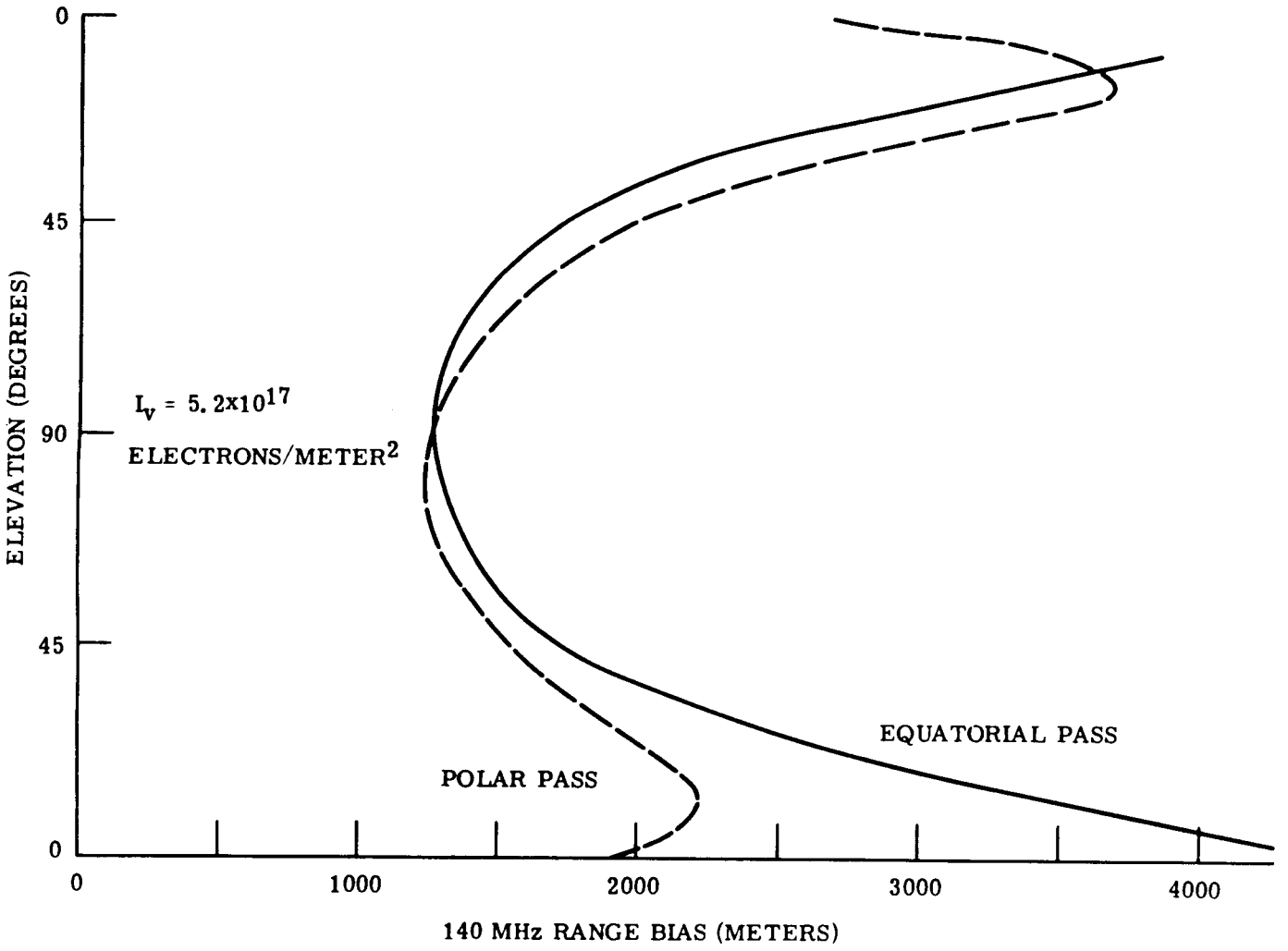

Figure 13

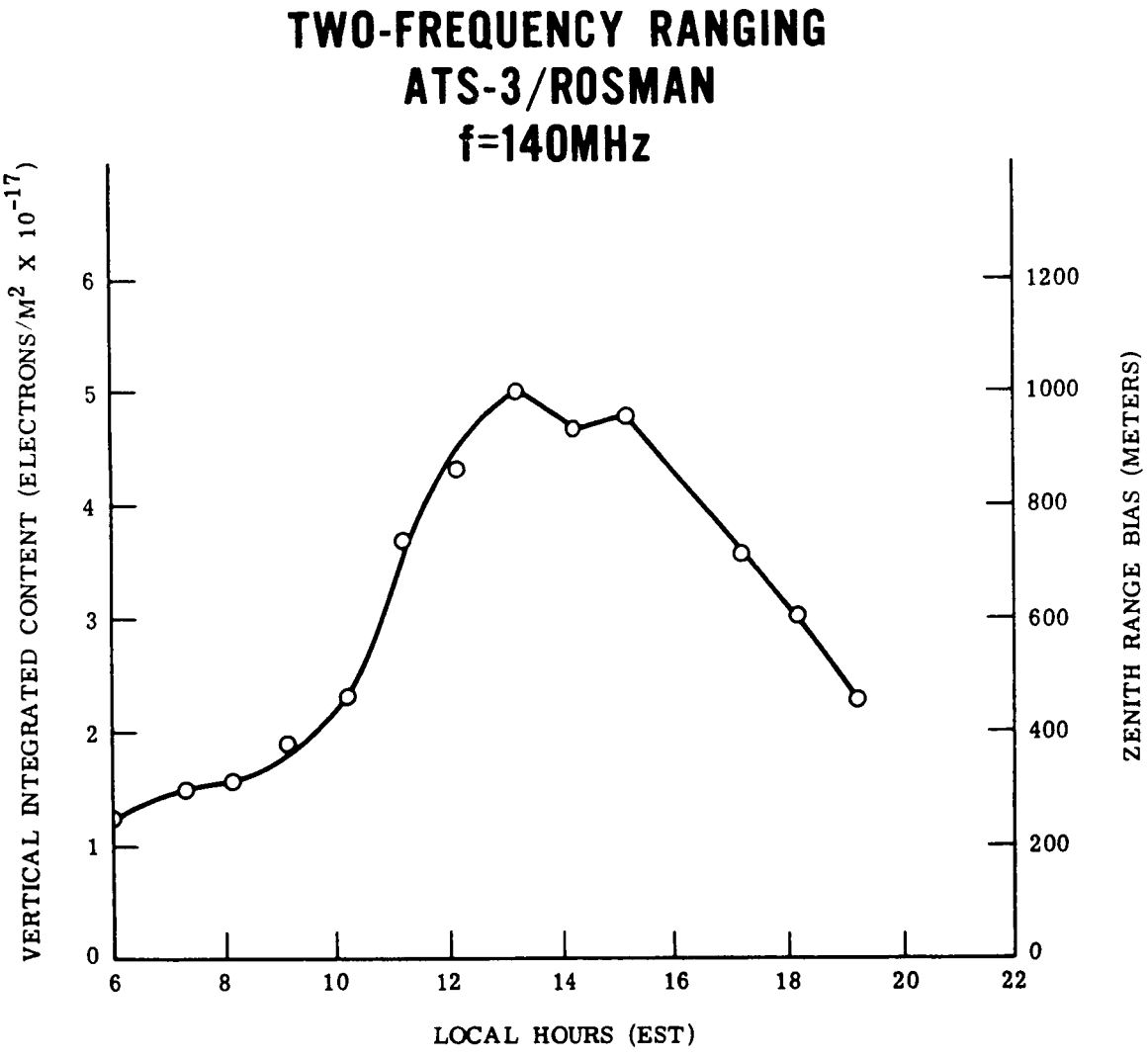
TWO-FREQUENCY RANGING
ATS-3/ROSMAN
f=140MHz
VERTICAL INTEGRATED CONTENT (ELECTRONS/M^2 x 10^{-17})
ZENITH RANGE BIAS (METERS)
LOCAL HOURS (EST)
0
1
2
3
4
5
6
0
200
400
600
800
1000
1200
6
8
10
12
14
16
18
20
22

Figure 14

the geostationary satellite ATS-3. The ionospheric diurnal effect is clearly traced out and the vertical total integrated content is calculated from the range difference data using equations 12 and 13.

3.4 FARADAY ROTATION MEASUREMENTS

Another widely used technique for observing integrated electron content is by means of Faraday rotation measurements. Once the ambiguity has been resolved, a continuous record of total vertical integrated content is available. Again this value of total electron content accuracy is subject to certain much discussed qualifying approximations (Ref. 36, 37, 38 and 39). However the basic scheme is as follows.

The Faraday rotation of the plane of polarization of a linearly polarized wave is given by the well known expression

$$\Omega = \frac{0.0297}{f^2} \int_0^{h_s} N(h)\, M\, dh \quad \text{Radians} \tag{19}$$

where $M = H \cos \theta \sec i$

- f = frequency of the wave
- $N(h)$ = electron density at a height h in the ionosphere
- H = the geomagnetic field intensity in MKS units
- θ = the angle between the ray and the geomagnetic field at the height h
- i = the angle between the ray and the vertical at the height h
- h_s = vertical height of the satellite

It is possible to approximate equation (19) by

$$\Omega = \frac{0.0297}{f^2} \overline{M} \int_0^{h_s} N(h)\, dh \quad \text{Radians} \tag{20}$$

where $\overline{M}$ is the value of M at some ionospheric height chosen so as to make equations (19) and (20) numerically most equivalent. In many calculations the value of $\overline{M}$ is chosen to be that of M at a height near 400 km along the ray path.

A typical record of Ω, the polarization rotation, is shown in Figure 15. This particular data was observed at GSFC on 25 February 1970 and during the solar eclipse of 7 March 1970 (Ref. 40).

In this GSFC test Faraday rotation of the ATS-3 VHF signals was recorded by means of a two channel phase lock receiver, each channel having as an input one of the two circular components derived from the incoming linear polarization. The linearly polarized signal is resolved into right and left hand circular components and then multiplied in an electronic phase detector whose full scale output is 2π radians where each π of rotation in spatial angle ϕ results in one cycle of electrical phase output. The Smyth Research Associates (SRA-524) receiver output, as shown in Figure 16, was recorded directly by an Esterline Angus chart recorder running at a rate of 1.5 inches per hour.

As shown in the records presented in Figure 15, during a normal day (such as February 25, 1970) ionization increases steadily during the morning hours up to the afternoon peak and then decays steadily as solar illumination decreases. Again with reference to Figure 15, a pronounced phase reversal occurred during the eclipse as the lunar shadow intercepted the line-of-sight between the GSFC site and ATS-3 and ionization abruptly decreased. At approximately 1400 hours local time the integrated electron content again increased up to the usual diurnal reversal.

Figure 17 indicates the observed variation in total electron content which can be expected over any given month. This type of data clearly establishes the need for solar flux updating if accurate ionospheric modeling is desired. As indicated in Figure 4 this capability has been provided in the NASA-GSFC model. The dotted line in Figure 4 for measured Faraday rotation and/or $f_0 F_2$ input indicates an alternate option for improving worldwide predicted ionospheric effects.

Figure 18 indicates the generally good agreement noted between modeled and measured integrated content extremes over a given month (Ref. 10). The measured data was obtained from Stanford as recorded in 1968 during the peak of the solar cycle.

It should be pointed out that orbit computation typically involves the use of several days of tracking data with each day including coverage from several stations. Hence ionospheric corrections must be good "on the average". That is, the residual variations implied by, for example, Figure 18 are even further smoothed by the trajectory fitting process.

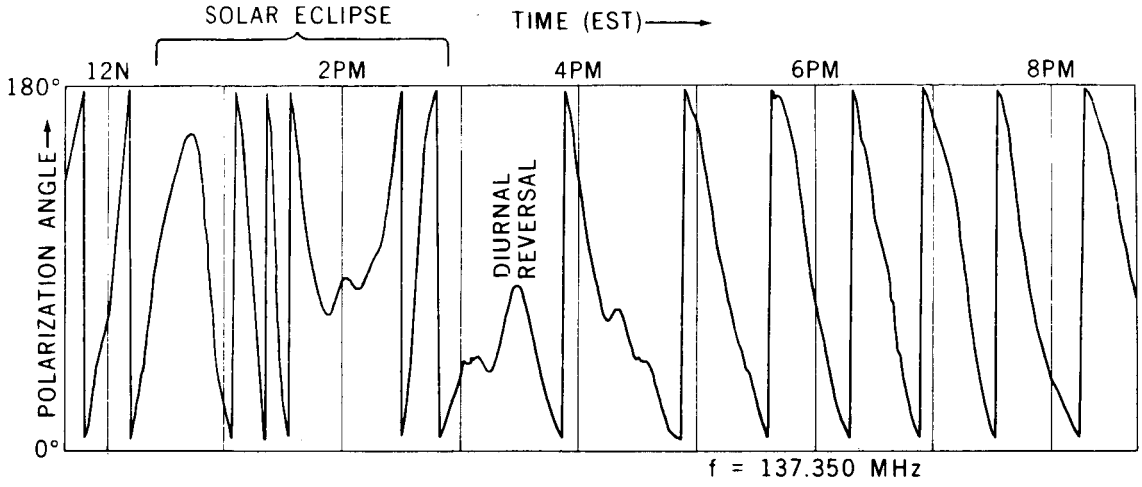

FARADAY ROTATION FROM ATS-3
SOLAR ECLIPSE OF 7 MARCH 1970

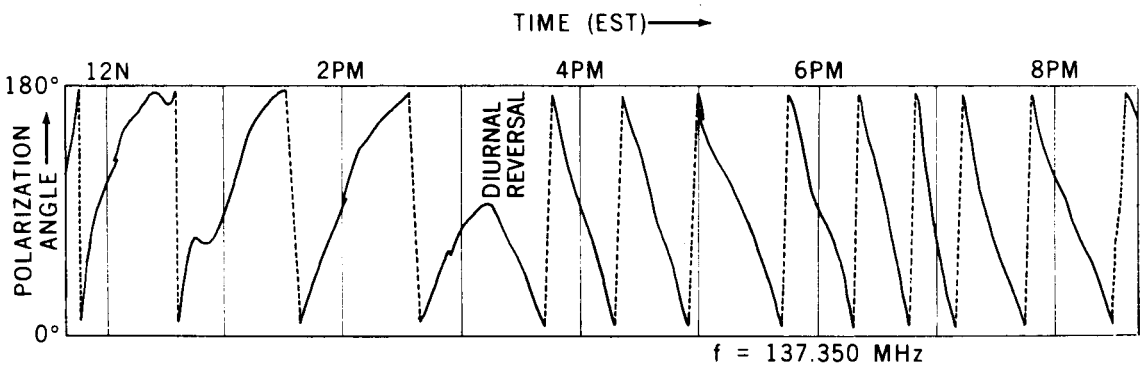

FARADAY ROTATION FROM ATS-3
TYPICAL DIURNAL REVERSAL
(DATA RECORD OF 25 FEBRUARY 1970)

Figure 15

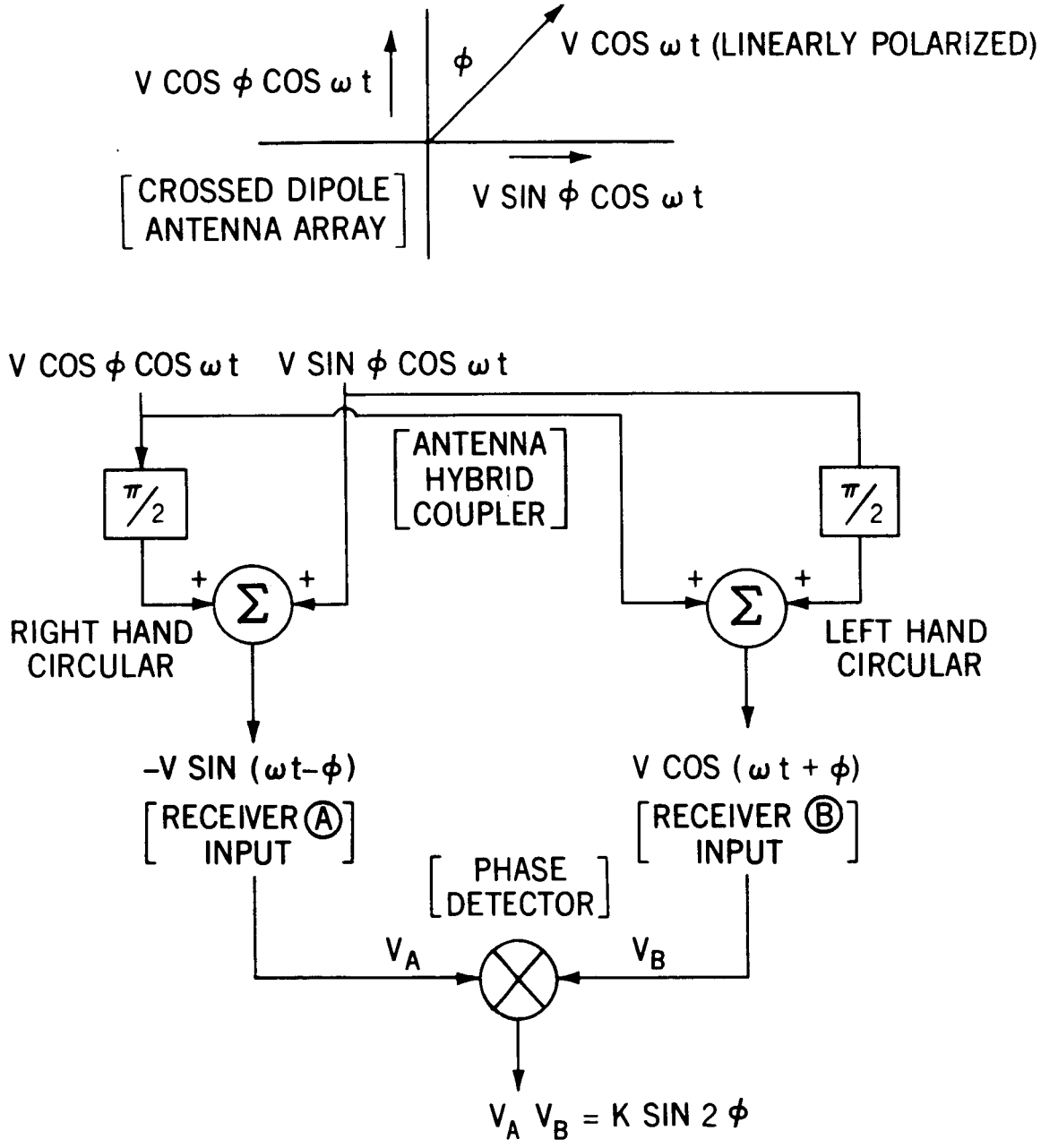
V COS φ COS ω t
φ
V COS ω t (LINEARLY POLARIZED)
[CROSSED DIPOLE ANTENNA ARRAY]
V SIN φ COS ω t
V COS φ COS ω t
V SIN φ COS ω t
[ANTENNA HYBRID COUPLER]
π/2
π/2
+
+
Σ
+
+
Σ
RIGHT HAND CIRCULAR
LEFT HAND CIRCULAR
-V SIN (ω t-φ)
V COS (ω t + φ)
[RECEIVER Ⓐ INPUT]
[RECEIVER Ⓑ INPUT]
[PHASE DETECTOR]
V_A
V_B
V_A V_B = K SIN 2 φ

Figure 16

After J. A. Klobuchar
September 1969 (Reference 41)

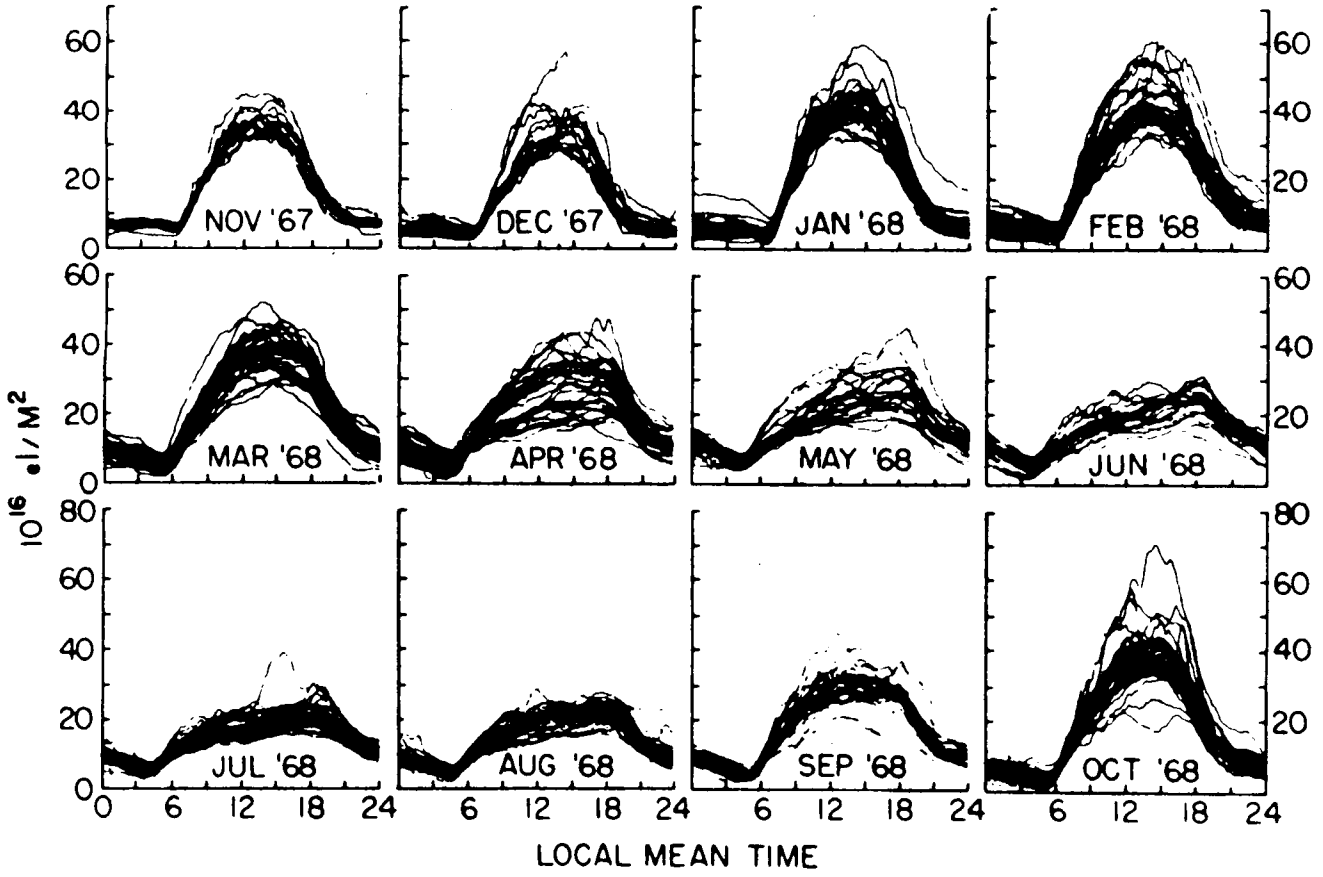

TOTAL EQUIVALENT VERTICAL ELECTRON CONTENT FROM HAMILTON, MASS. (Looking towards ATS-3).

Figure 17

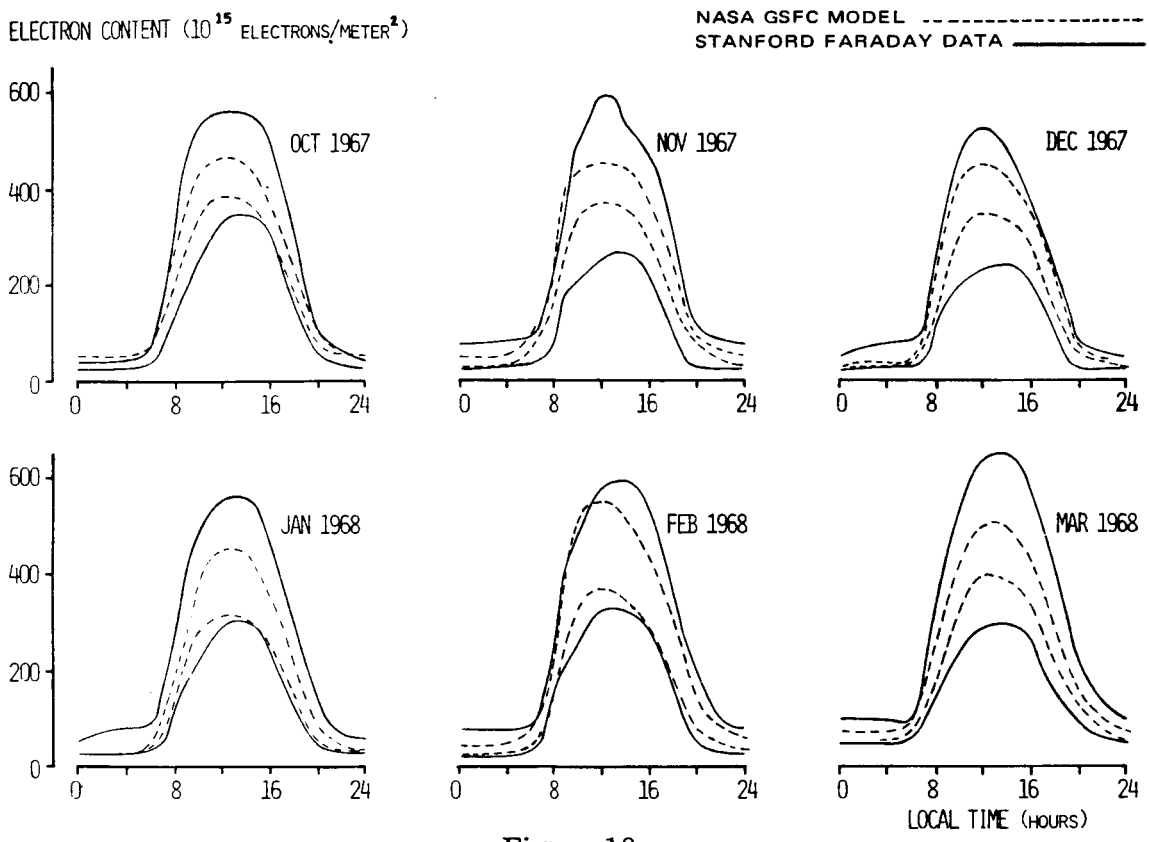

Figure 18

3.5 TRAJECTORY ANALYSIS

The range data is generally the most affected data type during any trans-ionospheric propagation. The bias is directly proportional to intervening electron content and independent of satellite motion. Therefore one method of viewing trajectory improvement is to calculate the RMS range residuals over a given data arc, comparing trajectories computed with and without ionospheric corrections. If VHF tracking is considered then the tropospheric range bias will be typically orders of magnitude less than the ionospheric bias. That is, the frequency independent tropospheric radio frequency bias at zenith is on the order of 2 to 3 meters and is also to a large extent modeled out (Ref. 42). Table 2 shows the significantly improved range data residuals during two typical orbit computations for the AIMP-E and IMP-G satellites. Individual values of ionospheric range bias during specific tracking station coverage times will vary from 50 meters to several kilometers depending on time of day, geographical location, aspect angle and so on.

Another means of detecting trajectory accuracy improvement is by means of trajectory overlap computations. Table 3 shows two seven day IMP-G satellite data arcs overlapped and compared again with and without the NASA-GSFC

Table 2
Goddard Trajectory Determination System
Test of NASA-GSFC Ionosphere Model

Spacecraft	VHF GRARR Tracking Date	Length of Arc	RMS Range Residuals (Meters)	
			No Ionosphere Model	Ionosphere Model
AIMP-E (Lunar Orbit)	Feb 25, 1972	3 Days	451	140
IMP-G	Oct 18, 1971	6 Days	410	200

Table 3
Orbit Accuracy Analysis

Position Difference of Overlapping Arcs			
	Maximum (km)	Minimum (km)	RMS (km)
No Atmospheric Correction	7.4	0.4	2.0
Atmospheric Correction Applied	2.5	0.3	0.7

Note:
1. Tracking of IMP-G at nominal 140 MHz
2. Data Span 9 Nov. to 19 Nov. 1970
3. Two seven day overlapping arcs compared
4. Range and range rate tracking from 5 stations

Ionospheric Model. In this case the RMS of the absolute position difference relative to an Earth Centered Coordinate system was computed for the two overlapped arcs. This measure of accuracy indicates an RMS error of 2.0 km without the model reduced to 0.7 km with the ionospheric model. The maximum difference was reduced from 7.4 km to 2.5 km. This is a marked improvement considering the fact that other modeling errors are present such as those associated with gravitational uncertainties, solar pressure uncertainty and station location errors.

4.0 CONCLUDING REMARKS

The NASA-GSFC Ionospheric Model for satellite tracking data corrections is part of the ongoing radio science and applications work being performed by the Geodynamics Program Division - GSFC to improve orbit computation accuracy. The NASA-GSFC ionospheric model as implemented in the operational support of the Radio Astronomy Explorer-B (RAE-B) has proven to be highly successful in improving data quality and hence trajectory accuracy.

It cannot be overstressed that this work is simply an extension and practical application of work performed by numerous researchers beginning perhaps with the first sun spot observers in 1775! Although this ongoing NASA effort is primarily directed toward satellite tracking data improvement it also has direct application to such important topics as:

- Correlation of ionospheric radio effects with satellite atmospheric drag modeling
- Very Long Baseline Interferometry radio star refraction correction
- Conventional radio astronomy refraction correction
- Measurement of interplanetary plasma based on group-phase phenomena
- Worldwide continuous predictions for 3 to 30 MHz skywave radio communications
- Solar geophysical research

REFERENCES

1. General Dynamics, "Goddard Range and Range Rate System - Final Project Report" General Dynamics Report R-70-010, 30 March 1970.

2. Nupen, W., "Bibliography on Ionospheric Propagation of Radio Waves (1923-1960)", NBS Technical Note No. 84, U. S. Dept. of Commerce, October, 1960.

3. Davies, K., "Ionospheric Radio Propagation" NBS Monograph 80, 1965.

4. Bremmer, H., "Terrestrial Radio Waves" Elsevier Publishing Co., 1949.

5. Kelso, J. M., "Radio Ray Propagation in the Ionosphere", McGraw-Hill, 1964.

6. Salaman, R. K., "Historical Survey of Fading at Medium and High Radio Frequencies", NBS Boulder Laboratories Technical Note No. 133, January 1962.

7. National Academy of Sciences, IGY Bulletin, Number 4, October 1957.

8. Kazantsev, A. N., "Absorbtion of Radio Waves in the Ionized Layers of the Atmosphere", TR IRE AN SSSR 2, 36, 1956.

9. Horner, F., and R. B. Bent., "Measurement of Terrestial Radio Noise", Proc. Roy. Soc. A 311, 527-542 (1969).

10. Bent, R. B., S. K. Llewellyn and P. E. Schmid "Ionospheric Refraction Corrections in Satellite Tracking", Space Research XII - Akademie-Verlag, Berlin, 1972.

11. Sterling, W. T., "A Study of the Effects of Atmospheric Refraction Corrections on Orbit Determination", Computer Sciences Corporation for NASA-GSFC under contract NAS5-11790 task number 146, April 1973.

12. U. S. Department of Commerce - NBS, "Ionospheric Radio Propagation" Circular 462, June 25, 1948.

13. Jones, W. B., "Atlas of Fourier Coefficients of Diurnal Variation of f_oF_2" NBS Technical Note No. 142, April 1962.

14. U. S. Department of Commerce-NBS, "Instructions for the Use of Basic Radio Propagation Predictions", Circular 465, August 27, 1947.

15. Hinds, M. E. and W. B. Jones, "Computer Program for Ionospheric Mapping by Numerical Means" NBS Technical Note No. 181, 20 August 1963.

16. Jones, W. B. and R. M. Gallet, "Ionospheric Mapping by Numerical Means", Published in Telecommunication Journal, No. 12, December 1960.

17. U. S. Department of Commerce, "Ionospheric Predictions", Telecommunications Research and Engineering Report 13, Volumes 2 through 4, September 1971.

18. Ostrow, S. M., "Handbook for CRPL Ionospheric Predictions Based on Numerical Methods of Mapping", NBS Handbook 90, 21 December 1962.

19. Jones, W. B. and R. M. Gallet, "Methods for Applying Numerical Maps of Ionospheric Characteristics", p. 649-662, Journal of Research of the National Bureau of Standards, D-Radio Propagation Vol. 66 D No. 6, Nov-Dec. 1962.

20. Beynon, W. J. G. and S. Rangaswamy, "Electron Collision Frequency in the F-Region of the Ionosphere" Nature Vol. 218 No. 5148, June 29, 1968.

21. Silberstein, R., "The Origin of the Current Nomenclature for the Ionospheric Layers", Journal of Atmospheric and Terrestrial Physics, Vol. 13, p. 382, 1959.

22. U. S. Department of Commerce, "Ionospheric Predictions" Telecommunications Research and Engineering Report 13, Volume 1, September 1971.

23. Hartree, D. R., "The Propagation of Electromagnetic Waves in a Refracting Medium in a Magnetic Field", Proc. Camb. Phil. Soc. 27: p. 143-161, 1931.

24. Lawrence, R. S., C. G. Little, H. J. A. Chivers, "A Survey of Ionospheric Effects upon Earth-Space Radio Propagation" Proc. IEEE, January 1964.

25. Appleton, E. V. and W. J. G. Beynon, Proc. Phys. Soc. 52 Pt. 1, 518, 1940.

26. Schmid, P. E., "The Conversion of Fundamental Tracking Data to Metric Form", NASA-GSFC X-551-69-3, January 1969.

27. Mallinckrodt, A. J., H. C. Parker, J. H. Berbert, "Analysis of Ionospheric Refraction Error Corrections for GRARR Systems", NASA-GSFC X-552-71-170, April 1971.

28. Schwartz, M., "Information Transmission, Modulation and Noise", Chapter 3, McGraw Hill, New York, N. Y., 1959.

29. Tucker, A. J. "Investigation of Ionospheric Errors in the Doppler Shift of CW Signals from Artificial Earth Satellites", Phd Thesis, Univ. of Texas, June 1967.

30. Schmid, P. E., "NASA MINITRACK Interferometer Refraction Corrections," NASA TN D-5966, March 1971.

31. Robinson, D. R., G. Nesterczuk, S. K. Llewellyn, and R. B. Bent, "Ionospheric and Tropospheric Corrections in GTDS", DBA Systems Inc. for GSFC under NAS5-11730, Sept. 1972.

32. Schleicher, L. H., S. K. Llewellyn, R. B. Bent "Tracking Data Relay Satellite System (TDRSS) VHF Propagation Study" Atlantic Science Corporation, June 1973.

33. Colin, L. and K. L. Chan, "Phase and Group Refractive Indices from the Collisionless Magnetoionic Theory", NASA TM X-1553, April 1968.

34. Weber, J., "Phase, Group and Signal Velocity", American Journal of Physics Vol. 22, No. 9, p. 618-620, December 1954.

35. Grenchik, T. J. and C. W. Murray, "Smoothing of Functions of Range and Range Rate Measurements from Earth Orbiting Satellites" NASA-GSFC X-551-72-385, October 1972.

36. Rao, N. N. and K. C. Yeh, "Comparison of Faraday and Doppler Methods of Obtaining Ionospheric Electron Content", JGR Space Physics, Vol. 73, No. 7, April 1, 1968.

37. Garriott, O. K., "The Determination of Ionospheric Electron Content and Distribution from Satellite Observations Part 1, Theory of the Analysis", JGR, Vol. 65, No. 4, April 1960.

38. Smyth, J.B., "Theory of Faraday Rotation and Differential Doppler Measurements", SRA Newsletter, No. 7, Smyth Research Associates, January 1968.

39. Da Rosa, A. V., "Radio Propagation Studies of the Ionosphere", Final Report, Radio Science Laboratory, Stanford University, NASA Contract NAS5-10102, February 1971.

40. Rangaswamy, S. and P. E. Schmid, "Measurement of Total Electron Content with a Geostationary Satellite During the Solar Eclipse of March 7, 1970", Radio Science, Vol. 6, nrs 8 and 9, Aug-Sept. 1971.

41. Klobuchar, J. A., "Propagation Delays of VHF Waves", AGARD Report No. 571, p. 89-92, August 1969.

42. Marini, J. W., "Correction of Satellite Tracking Data for an Arbitrary Tropospheric Profile", Radio Science Vol. 7, No. 2, February 1972.